MATRIX SHINGLE SOLAR MODULES: PILOT PRODUCTION FOR BUILDING-INTEGRATED PV APPLICATIONS

Torsten Rößler[1], Najwa Abdel Latif[1], Elmar Lohmüller[1], Daniel von Kutzleben[1], Norbert Kohn[1], Jale Schneider[1], Jonas De Rose[1], Sebastian Birnkammer[1], Martin Wiese[1], Marco Ernst[1], Felix Basler[1], Jacob Forster[1], Laura Stevens[1], John Morello[2], Gaetan Carrier[2], Achim Kraft[1], and Holger Neuhaus[1]
[1] Fraunhofer Institute for Solar Energy Systems, Heidenhofstr. 2, 79110 Freiburg, Germany
[2] Freesuns Solar Roofs, Chemin de la Séverire 6, 1114 Colombier, Switzerland

ABSTRACT: Building-integrated photovoltaics (BIPV) can decarbonize buildings by integrating solar modules directly into facades and roofs. However, conventionally stringed modules limit design flexibility and perform poorly under partial shading, which hinders widespread adoption. Matrix shingle modules solve these problems by distributing electrical connections and separating module geometry from wiring constraints. This approach provides design freedom and better shading tolerance. This paper describes scaling matrix shingle technology from laboratory to pilot production. We established a repeatable pilot process with defined quality controls and demonstrated improvements in yield and throughput throughout production phases. We quantified losses from cell to module level and identified realistic improvement opportunities. In our demonstration campaign, we produced and characterized 4500 modules. We validated technological breakthroughs through a challenging production run of 872 modules. By optimizing the terminal connection - switching the electrically conductive adhesive (ECA) and changing from dispensing to a brushing application - we reduced the B-grade module share from a critical 14.9% to just ~3%. This improvement increased first-pass yield and stabilized daily throughput above 150 modules. Representative modules achieved 14.9 W (20.1% efficiency) with edge passivation, outperforming conventional roof tile products. These results demonstrate that production-focused optimization, supported by modelling, can achieve stable, high-yield pilot production of matrix shingle BIPV modules while maintaining both power output and aesthetic appeal.

Keywords: BIPV, matrix shingle technology, pilot production, electrically conductive adhesive (ECA), shading tolerance, yield.

1 INTRODUCTION

1.1 Problem Statement and Relevance

Matrix shingle technology is an advanced interconnection method recognized for increasing power density and offering superior aesthetic uniformity and shading resilience, making it highly attractive for building-integrated photovoltaics (BIPV) [1]–[3]. However, the large-scale adoption of BIPV, which is necessary to meet climate goals [4], is hindered by a critical mismatch between the market's demand for customized, high-mix/low-volume production and the standard PV industry's high-volume/low-mix model.

This "Scale-Up Gap" is particularly acute for matrix shingling. Its industrial adoption requires the establishment of new, stable and scalable production processes. Against the backdrop of Europe's domestic PV manufacturing sector facing existential threats from a collapse in module prices to below 15 Euro-Cents/W, driven by global overcapacities and import pressure [5]–[7], the SPHINX EU project [8] was initiated to address this specific challenge by advancing matrix shingle technology towards industrial maturity.

1.2 Research Question and Objectives

To bring matrix shingle technology to an industrial scale, promising laboratory results must be converted into a stable, scalable, and economically viable manufacturing process. While the fundamental advantages of the technology are established [3], [9], the primary challenges lie in increasing throughput and the control of process-material interactions at an industrial pilot scale.

This work therefore aims to identify the key parameters for a successful production transfer by pursuing two primary objectives:

1. To establish a repeatable pilot process and use a transparent, physics-based model to quantify the power losses from cell to module.
2. To identify and optimize the dominant material-process interaction for the ECA-based terminal connection to maximize production yield and process stability.

2 METHODOLOGY

To address the identified scale-up gap, a systematic methodology was developed. It combines a flexible pilot production line with a simulation-supported loss analysis and a large-scale validation campaign.

2.1 Matrix Shingling Pilot Line at Fraunhofer ISE

The experimental work was conducted on a dedicated matrix shingling pilot production line for BIPV products at Fraunhofer ISE, established within the SPHINX project [9]. The line is specifically designed to bridge the gap from laboratory concepts to industrially relevant volumes, targeting the high-mix/low-volume requirements of the BIPV market.

Its hybrid architecture combines automated key processes with flexible manual workstations to accommodate a wide range of custom BIPV form factors.

Figure 1: Layout of the matrix shingling pilot line at Fraunhofer ISE, including shingle cutting (Fyoda), automated assembly (M10 Shirkan), lamination (Bürkle Ypsator), and *I-V*/EL testing (Halm). Host cell characterization and edge passivation are performed off-line.

The main process sequence, illustrated in Figure 1, includes:

1. Shingle cell cutting (Fyoda)
2. Cut edge passivation (PET) [10] (performed off-line)
3. Automated matrix assembly (M10 Industries Shirkan Stringer)
4. Manual layup
5. Terminal connection / bussing
6. Lamination (Bürkle Ypsator)
7. Junction box attachment
8. Final electrical and optical characterization (Halm IV/EL Tester)
9. Labelling and packaging

For this study, the line was configured to produce the solar roof tiles for project partner Freesuns, demonstrating a stable capacity of 2.4 MWp/a in a two-shift, five-day-a-week model. The line's theoretical peak capacity is estimated at up to 18.5 MWp/a, achievable through continuous operation and a shift to larger, high-efficiency module formats.

2.2 The Solar Roof Tile Demonstrator

The product manufactured and analyzed in this study is a matrix-shingled solar roof tile, co-developed with project partner Freesuns. The tile, shown in Figure 2, has outer dimensions of 510 mm × 450 mm and features a glass-glass configuration.

The electrically active area is composed of a matrix of TOPCon solar cell shingles. Specifically, each module integrates ten electrically active full-sized shingles (210 mm × 26 mm) and six half-sized shingles (105 mm × 26 mm). This arrangement was specifically engineered to yield the current-voltage (*I-V*) characteristics required for seamless integration into the planned rooftop PV system topologies.

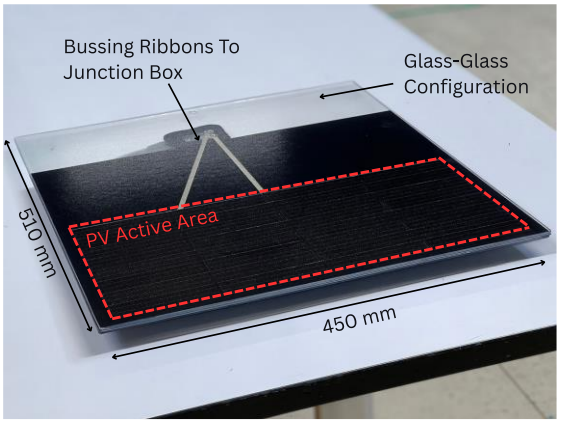

Figure 2: Matrix-shingled solar roof tiles co-developed with Freesuns. The tile consists of ten electrically active full-sized shingles" (210 mm × 26 mm) and six "half shingles" (105 mm × 26 mm). A pilot run of 4500 units confirmed repeatable manufacturing yield.

2.3 Large-Scale Validation and Process Control

To validate the manufacturing process, a large-scale campaign was executed to produce approximately 4500 solar roof tiles for the project partner Freesuns. Production was organized into discrete batches to align with the delivery schedules for three distinct demonstrator projects (e.g., “Pully”, “Arzier”). While primarily a logistical necessity, this batch structure provided a clear framework for assessing process stability and material performance over time.

Process control relied on systematic data logging and end-of-line characterization. The in-house SmartCell software ecosystem was used to log production data and ensure material traceability [11]. The core of the quality assessment was the electrical and optical characterization (*I-V* and EL measurement) of every module. Modules were classified based on their maximum power P_{MPP} according to strictly defined quality gates, specified in alignment with the project partner Freesuns:

- Grade A (Accept): $P_{MPP} > 14.25$ W
- Grade B (Reduced Power): $10\ W \leq P_{MPP} \leq 14.25$ W
- Grade C (Scrap): $P_{MPP} < 10$ W

The systematic tracking of these module grades per batch was critical. It enabled the quantitative detection of the significant yield degradation that occurred during the campaign and triggered the root-cause analysis detailed in Section 3.

2.4 Cell-to-Module (CTM) Power Loss Modelling

To deconstruct the power loss chain from host cell to final module, a physics-based CTM model was developed. The model's primary goal was to reproduce the measured median power and distribution of the production modules, thereby validating the quantification of individual loss mechanisms.

The model is built on a Monte Carlo framework. The simulation starts by generating a statistical population of solar cells whose *I-V* parameters and variance are fitted to measured data from three distinct stages: the initial host cells, the shingles directly after laser cutting, and the shingles after edge passivation using the passivated edge technology (PET) [10]. The model explicitly accounts for the geometry of half-size shingles by scaling the parameters accordingly. To ensure the model represents the bulk of the manufacturing campaign, the simulation is intentionally based on the standard host cells (23.5% baseline efficiency with PET treatment) and explicitly excludes the limited batch of top-performing LECO-treated cells (laser-enhanced contact optimization). Subsequent processing steps are simulated by applying dedicated physical or analytical sub-models.

A key focus was the detailed simulation of the shingle interconnection. Instead of using simplified lumped resistances, the full *I-V* curves of the individual shingles within the matrix are numerically and robustly added. This sophisticated approach accurately captures complex electrical mismatch effects.

The parameterization of the overall model is based on a combination of sources. Where possible, direct process measurements were used. For parameters that were not directly accessible during production, such as the ECA contact resistance and the finger conductivity of the host cells, values were derived from a combination of literature data and internal empirical knowledge (e.g., [12], [13]).

3 RESULTS

3.1 Cell-Level Process Optimisation

The starting material for module production were industrial TOPCon host solar cells in the G12R-format (210 mm × 182 mm), featuring a customized busbar design for shingling. The baseline efficiency of these cells was (23.5±0.2)%. To optimize cell performance for the shingling process, two additional treatments were implemented and evaluated.

First, laser-enhanced contact optimization (LECO) was applied to a subset of cells to reduce contact resistance [14]. This process step demonstrated a significant efficiency gain of approximately $0.8\%_{abs}$, resulting in a cell efficiency of 24.3%. Due to limited tool capacity, LECO was not applied to the majority of the production volume but served to define the upper performance limit.

Second, PET was consistently implemented after cell separation. This treatment mitigates edge-related recombination losses inherent to the cutting process [15], [16]. PET reliably recovered about $0.5\%_{abs}$ of the efficiency loss caused by cell separation.

Shingle cells treated with PET alone, which constituted the bulk of the production, achieved a stable efficiency in the range of 23.0% to 23.4%. These optimized cells established a consistent and high-quality performance baseline for the subsequent module fabrication and loss analysis.

3.2 Overall Production and Throughput Analysis

Between March and August 2025, a large-scale pilot production campaign was executed to demonstrate the manufacturing readiness of the matrix shingle technology for BIPV applications. A total of 4500 solar roof tile modules were produced for four different installation sites in Switzerland, in collaboration with our project partner Freesuns.

A significant increase in daily output is observable in the later stages of the campaign. This was primarily achieved by identifying and mitigating a key production bottleneck. An analysis of the individual station throughputs identified the lamination process as the primary constraint, as shown in Table I.

Table I: Throughput analysis for the solar roof tile production, identifying the lamination process as the line's bottleneck.

Process Step	Throughput (units per hour) specifically for Freesuns’ PV roof tile
Shirkan Stringer	25
Lamination	16
Final Electrical Test	24

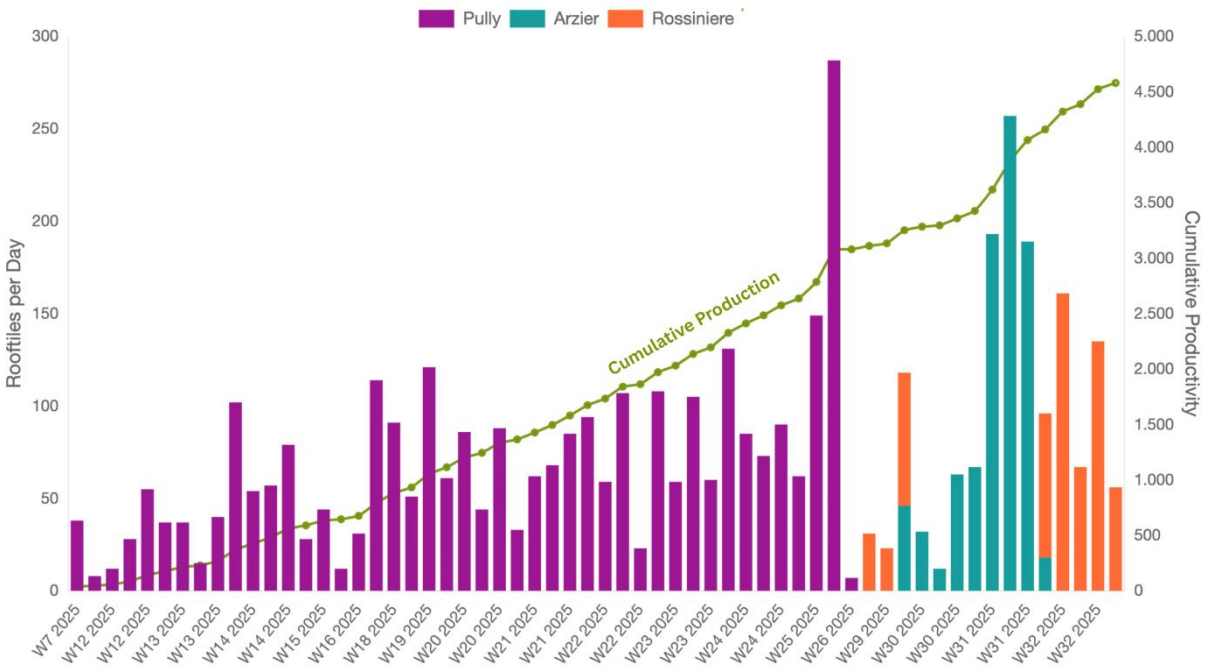

Figure 3: Throughput and cumulative output during the March–August 2025 campaign. The switch to ECA 2 with brushing increased first-pass yield, and commissioning of a second laminator stabilized throughput above ~150 modules/day.

With a capacity of 16 modules/hour, the laminator's throughput was significantly lower than that of upstream and downstream processes. The commissioning of a second lamination tool effectively doubled the capacity of this process step, allowing the daily throughput to stabilize at a level exceeding 150 modules per day (with one shift). Eliminating the lamination bottleneck through parallel processing demonstrated that the line's throughput is not intrinsically limited by this step and provided a clear path for further scaling of the production volume.

3.3 Identification of the Key Yield Bottleneck

Despite the successful ramp-up in production volume, a critical quality issue emerged during the manufacturing of the “Arzier“ demonstrator batch, which significantly impacted the production yield. While the initial “Pully“ demonstrator batch showed a high A-grade rate of 92.8%, the subsequent "Arzier" batch suffered from a sharp decline in quality.

This is quantitatively demonstrated in Figure 4, which compares the quality distribution across the production campaigns. The share of B-grade modules for the “Arzier“ batch increased to an unacceptable level of 14.9%. Root cause analysis identified the ECA interconnection as the source of this yield loss. The initial process relied on a manual dispensing of ECA 1 onto the rear side of the terminal shingle rows, a method that proved difficult to control. During the subsequent lamination process, the applied pressure caused this uncured adhesive to smear and make contact with the cell edge. This excess, conductive material then formed parasitic electrical shunts, leading to a significant reduction in the modules' power output.

This failure mode is clearly visualized in the electroluminescence (EL) image in Figure 5 (bottom left), which shows a characteristic dark area where a shunt has occurred. The corresponding power distribution for this production batch shows a distinct tail towards lower power values, which accounts for the high B-grade share. This material-process interaction represented the single most critical bottleneck for achieving a stable, high-yield production.

3.4 Yield Recovery through Terminal Bussing Optimization

To address the critical yield bottleneck, a two-part process optimization was implemented, targeting both the ECA material and its application method. This involved two key changes:

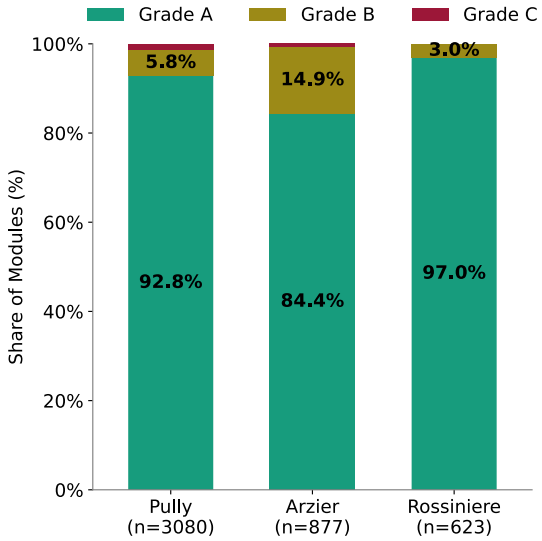

Figure 4: Distribution of A-, B-, and C-grade modules across three successive production campaigns. The high B-rate in the **“**Arzier**“** campaign triggered a process optimization. The success of this change is demonstrated by the recovery to a high A-rate of >97% in the subsequent **“**Rossinière**“** campaign.

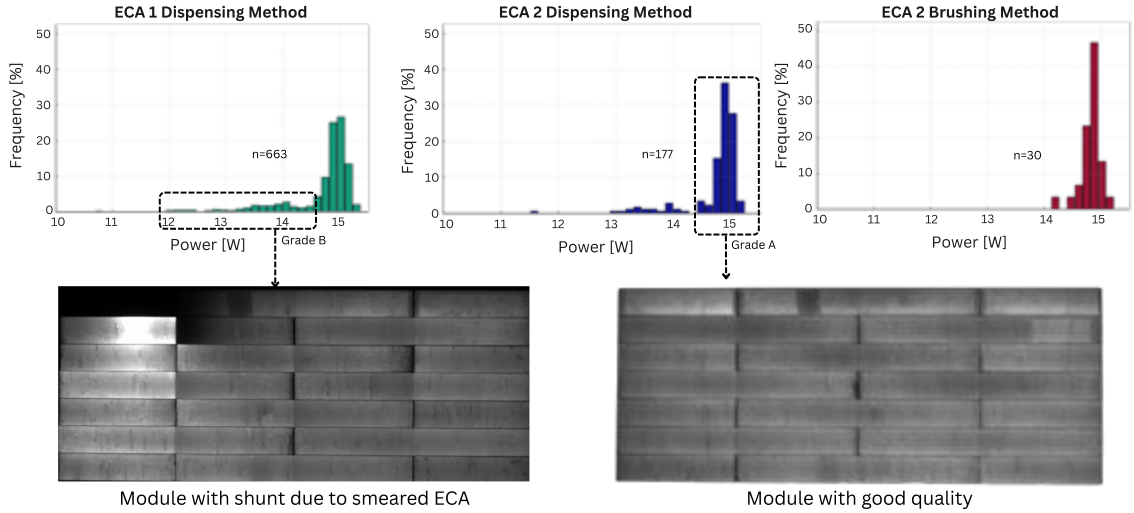

Figure 5: Comparison of module P_{MPP} distributions for sequential phases of the Arzier batch. The process change from ECA 1/dispensing to ECA 2/brushing reduced the left-tail spread and shifted the median to higher P_{MPP} values, lowering the B-grade fraction from 14.9% to ~3%. Characteristic shunting failures are visible in the corresponding electroluminescence image

1. Material Change: The initial ECA (ECA 1) was replaced by an alternative (ECA 2) with curing kinetics better suited to the thermal budget of the lamination process. While the ECA 1 is an established material for shingle-to-shingle interconnection, its longer curing time in this specific terminal bussing application allowed it to remain liquid under pressure and heat, causing the observed smearing.
2. Application Method Change: The manual, difficult-to-control dispensing process was replaced with a manual brushing technique. The brushing technique proved to be a more intuitive and controllable manual process, enabling operators to consistently apply a thin, uniform adhesive layer onto the terminal shingle row.

This optimized material-process combination immediately eliminated ECA smearing, leading to a significant and instantaneous yield recovery. The B-grade share plummeted from 14.9% in the "Arzier" batch to just ~3% in the subsequent "Rossinière" batch, which was produced entirely with the new method. This improvement is directly visible in the module characteristics shown in Figure 5: the optimized process resulted in a tight power distribution centered at 14.9 W - eliminating the previous low-power tail - and a perfectly uniform, shunt-free EL image. This robust method was subsequently adopted as the new production standard.

3.5 Final Module Characteristics and Reduced Performance Variability

With the optimized terminal bussing process established, the electrical characteristics of the modules were analyzed to validate the final product quality and the stability of the manufacturing process.

Representative Grade A modules, produced with the robust method, achieve a median maximum power of 14.9 W. Based on the active cell area of 0.0742 m², this corresponds to a module efficiency of 20.1% under standard testing conditions (STC). The median fill factor (*FF*) for these modules was consistently measured in the range of 73.5% to 74.0%. This value, noticeably lower than the >80% typically expected from TOPCon modules with optimized metallization, is primarily attributed to a non-optimized finger metallization on the host cells and missing LECO used for this batch and is explicitly not a result of the interconnection process itself, which shows minimal resistive impact as confirmed by the CTM analysis.

A key outcome of the process optimization was the significant reduction in performance variability. The power distribution histograms in Figure 5 clearly demonstrate a distinct narrowing of the statistical spread for modules produced after the process change. The long, low-power tail characteristic of the initial process was effectively eliminated. This confirms that the new bussing method not only removed the critical shunt-related failure mode but also resulted in a more consistent and repeatable electrical quality for all A-grade modules.

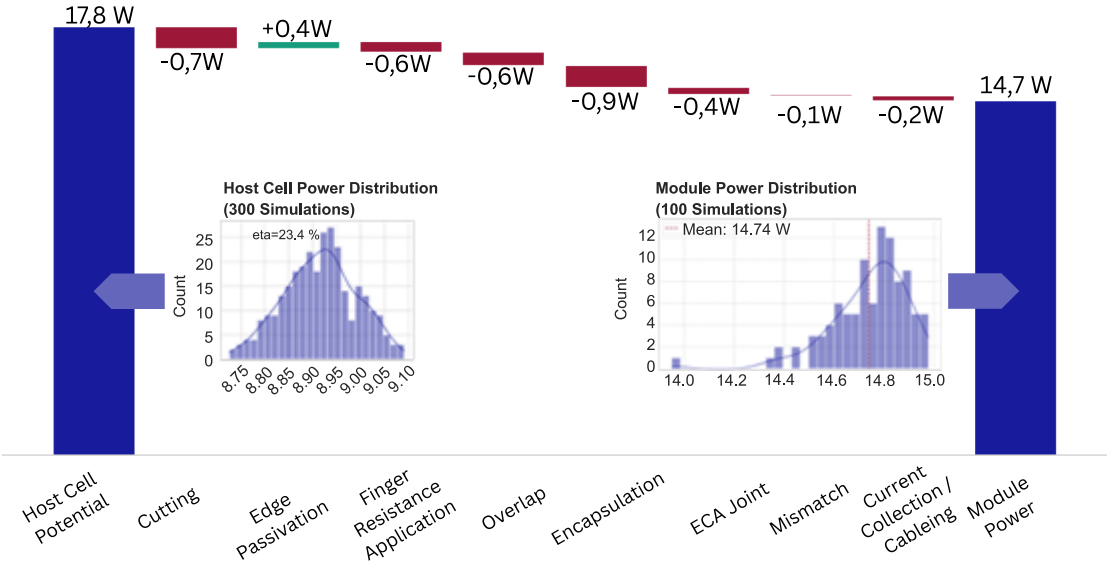

Figure 6: Waterfall chart of cell-to-module (CTM) power losses. The simulation starts from the average host cell power potential of 17.8 W (23.4% efficiency) representative of the main production campaign. By modeling successive process steps, the simulation calculates a final median module power of approximately 14.7 W. This result is in excellent agreement with the experimentally measured median power of 14.9 W for the normal production batches and thus validates the model's underlying physical assumptions. The primary purpose of this CTM analysis is not to perfectly predict the output of a single batch, but to confirm that all significant power loss mechanisms from cell to module have been correctly identified and quantified.

A detailed cell-to-module (CTM) loss analysis provides the broader context for this final module performance. As illustrated in the waterfall chart in Figure 6, the model employs a Monte Carlo approach to break down the power loss pathway from the initial host cell potential to the final measured module power, accounting for process-induced variations. The simulation, which accurately reproduces the measured median power, identifies the cell cutting process (−0.7 W) and the encapsulation (−0.9 W) as the two largest individual loss contributors. While the edge passivation step successfully recovers a significant portion of the cutting losses (+0.4 W), other factors such as increased resistive losses in the finger metallization (−0.6 W) and optical shading from the shingle overlap (−0.6 W) further reduce the power output. In contrast, losses from the interconnection technology itself, such as the ECA joint resistance (−0.4 W) and cell-to-cell mismatch (−0.1 W), are comparatively low, demonstrating the high quality and low resistive impact of the implemented interconnection process.

Figure 7. The “Pully” demonstrator showcases the final application of the matrix shingle solar roof tiles. The seamless aesthetic integration validates the success of the high-yield pilot production process.

4 DISCUSSION

The results of this work demonstrate the resolution of a critical yield issue that exemplifies the challenges of industrial scaling. The yield drop during the “Arzier” production batch to an 14.9% B-grade share was not a simple equipment failure, but a systemic flaw: a process step that was not sufficiently controlled and whose inherent weakness was exposed by our upscaling efforts. The root cause was a fundamental mismatch between material properties and process parameters: the initial ECA (ECA 1) requires 6−7 minutes to cure at 145 °C. During this time, the adhesive remained liquid, allowing the applied lamination pressure to cause it to flow and create electrical shunts. In contrast, the selected alternative (ECA 2) cures within 30 seconds at the same temperature. It therefore solidifies almost instantly, preventing any flow when the laminator applies pressure and thus reliably eliminating the failure mode. The CTM model provides a crucial context for this: by quantifying the theoretical loss chain, it shows that the inherent power losses from the interconnection technology itself (e.g., ECA joint resistance, mismatch) are minimal. This confirms that the observed yield crash was a preventable process defect, not a fundamental flaw of the matrix shingle technology.

This experience highlights two key principles for successful industrial upscaling: the necessity of continuous yield monitoring with rapid feedback loops, and the value of pragmatic, easily implementable solutions. The switch to a manual brushing technique exemplifies the latter; it was a highly effective and robust solution that was quickly adopted by operators and immediately stabilized the process. By applying this agile problem-solving approach, the process was fundamentally de-risked. This is evidenced by the sustained A-grade rate of over 97% and the increased throughput of over 150 modules/day, which enabled the successful production of all 4500 modules. This demonstrated stability is the prerequisite for a viable business case, lowering the barrier for industrial adoption. The successful real-world deployment of all 4500 modules culminated in several demonstrator projects. Figure 7 shows the final installation on the “Pully” demonstrator, validating not only the production process but also showcasing the seamless aesthetic integration that matrix shingle technology brings to buildings. This experience highlights a key principle for successful industrial upscaling: process stability is often limited not by the core technology itself, but by the nuanced interactions between materials and process parameters that only become apparent at scale.

While this study establishes a robust pilot-scale process, the transition to fully automated, high-volume manufacturing presents the next set of well-defined engineering challenges. The primary next step is the development of an automated application system for the terminal connections that replicates the quality of the manual brushing method at industrial speeds. Finally, the ultimate validation of the technology's reliability will come from the systematic analysis of long-term performance data from the demonstrator sites. This work provides the foundational process stability required to confidently pursue these next steps towards full industrialization.

5 CONCLUSION

We successfully transitioned matrix shingle technology to a stable, high-yield pilot production process capable of industrially relevant volumes. The resolution of a critical yield bottleneck, caused by an ECA-process mismatch, was the key achievement. By implementing a fast-curing adhesive and a robust application method, we reduced the B-grade module fraction from an unsustainable 14.9% to ~3%.

This process stabilization enabled a daily throughput exceeding 150 units and the successful manufacturing of the 4500-module demonstrator campaign. The resulting Grade A modules consistently achieve a median power of 14.9 W (20.1% efficiency). We have therefore retired the foundational process risks for matrix shingle technology at the pilot scale, providing a validated and quantitative basis for its future industrialization.

ACKNOWLEDGEMENTS AND DISCLAIMER

(Part of the) Results presented have been achieved within the SPHINX project. Funded by the European Union under grant number 101136094. Views and opinions expressed are however those of the author(s) only and do not necessarily reflect those of the European Union. Neither the European Union nor the granting authority can be held responsible for them.

REFERENCES

[1] D. von Kutzleben et al., Proceedings 8th World Conference on Photovoltaic Energy Conversion, (2022) 541.
[2] N. Abdel Latif et al., Proceedings 40th European Photovoltaic Solar Energy Conference & Exhibition, (2023) 1.
[3] N. Klasen et al., Progress in Photovoltaics: Research and Applications 30 (2022) 325.
[4] T. E. Kuhn et al., Energy and Buildings 231 (2021) 110381.
[5] Financial Times, (2025). [Online]. Available: https://www.ft.com/content/5f83760f-5da8-474c-81db-0c0dc3c6c8aa
[6] N. Ford, Reuters, (2024). [Online]. Available: https://www.reuters.com/business/energy/solar-suppliers-call-eu-aid-imports-crush-margins-2024-03-21/
[7] SolarPower Europe, EU Market Outlook for Solar Power 2024-2028, (2024). [Online]. Available: https://www.solarpowereurope.org/insights/outlooks/eu-market-outlook-for-solar-power-2024-2028/detail
[8] Project Website Horizon Europe Project Sphinx, Solar Photovoltaics Integrated into the Built Environment, Available: https://sphinxproject.eu/
[9] T. Rößler et al., SPHINX Deliverable report D3.4, (2024). [Online]. Available: https://sphinx-project.eu/publications/
[10] E. Lohmüller et al., Solar Energy Materials and Solar Cells 258 (2023) 112419.
[11] Fraunhofer ISE, Data Management in Database Networks with Metadata Models, [Online]. Available: https://www.ise.fraunhofer.de/en/business-areas/photovoltaics-production-technology-and-transfer/ai-and-data-management/data-management-in-database-networks-with-metadata-models.html
[12] M. I. Devoto et al., Solar Energy Materials and Solar Cells 262 (2023) 112518.
[13] J. Lossen et al., SiliconPV Conference Proceedings 2 (2024).
[14] T. Fellmeth et al., Progress in Photovoltaics: Research and Applications 30 (2022) 1393.

[15] P. Baliozian et al., IEEE Journal of Photovoltaics 10 (2020) 390.
[16] E. Lohmüller et al., Progress in Photovoltaics: Research and Applications 31 (2023) 729.